Quantitative Determination of Titanium Lattice Defects and Solid-State Reaction Mechanism in Iron-Doped TiO_2 Photocatalysts

J. A. Wang* and R. Limas-Ballesteros

Superior School of Chemical Engineering, National Polytechnic Institute, UPALM, 07738 Mexico City, Mexico

T. López, A. Moreno, and R. Gómez

Department of Chemistry, Universidad Autónoma Metropolitana-I, A. P. 55-534, 09340 Mexico City, Mexico

O. Novaro† and X. Bokhimi

Institute of Physics, National University of Mexico (UNAM), A. P. 20-364, 01000 Mexico City, Mexico

Received: December 7, 2000; In Final Form: June 27, 2001

Iron-doped titania photocatalysts with different iron contents were prepared by using a sol−gel method in acidic media. The crystalline structures of the various phases calcined at temperatures ranging from 70 to 800 °C were studied by using the Rietveld technique in combination with XRD experiments. The average crystallite size of the phases, lattice cell parameters, phase concentrations, and titanium cationic defects in the crystalline structures of different samples were quantitatively determined. Both iron content and calcination temperature strongly affected phase transformation and solid-state reaction mechanism. Below 400 °C of calcination, all the samples had some brookite and a majority of anatase phase. Iron ions were uniformly distributed in the interstices of titania crystals to form a titanium−iron solid solution when the samples were calcined at 80, 200, and 400 °C. However, when the temperature was 800 °C, Fe_2TiO_5 was produced in the sample containing 5 wt % Fe by a reaction between interstitial iron ions and lattice titanium ions, and in the 10 wt % Fe sample through a reaction of hematite with titania phases. The crystalline structures of titania phases were distorted at higher calcination temperature. For the first time, it is possible to show that titanium lattice defects related to the hydroxyl ions in the crystalline structures were created in anatase and rutile phases. The concentration of titanium defects remained almost constant below 400 °C but decreased as the calcination temperature was higher than 600 °C due to the decrease of the hydroxyls in the crystalline structure.

1. Introduction

To meet the increasingly stringent standards of environmental regulations, catalytic techniques are being applied in the fields of environmental protection. Photocatalysis is one technique that has great potential to control aqueous organic contaminates or air pollutants. It is believed to have several advantages over conventional oxidation processes, including (1) complete mineralization of the pollutants, (2) use of the near-UV or solar light, (3) no addition of other chemicals, and (4) operation at near room temperature.[1,2] Although photocatalyzed degradations of trace toxic organic compounds in liquid waste have been studied intensively in the past decade, there still remain some problems in practical applications.[3−7] Fundamental research regarding the improvement of photocatalyst performance, extension of the catalyst absorption to the visible range, or the use of a wider range of the solar spectrum are priorities to be developed.[8]

Titania is an attractive photocatalytic material in the control of toxic pollutants by means of gas−solid or liquid−solid photocatalyzed reactions.[9,10] However, the main crystallographic form of titania is anatase, which can only absorb light wavelengths shorter than 400 nm and generates a value of 3.2 eV of band gap energy. This limits its application. Another titania phase, rutile (3.02 eV, 411 nm), shows less activity than anatase. To utilize a wider range of the electromagnetic spectrum for photocatalysis, doped-TiO_2 is used with photosensitizers or semiconductors with smaller band gap energies, e.g., CdS and Fe_2O_3.[11−13]

It is well-known that phase transformation among brookite, anatase, and rutile are related to the thermal treatment. When the calcination temperature increases, phase transformation from brookite or/and anatase into rutile occurs irreversibly.[14,15] The crystallite structure of rutile is hence more thermally stable at high temperature. When titania is doped with other metal oxides, its properties are remarkably modified. For example, some dopants such as iron and vanadium can enhance the electrical transferring properties between titanium and iron or vanadium atoms, that change its electrical conductivity, optical, and hence catalytic properties when these materials are illuminated by the UV light.[16−18]

During thermal treatment, guest metal oxides or dopants may react with titania to form new crystalline phases. In the case of the Ti−Fe−O system, when the calcination temperature is up

* Author to whom correspondence should be addressed, Tel: (++52 5)7296000 ext. 55124. Fax: (++52 5)5862728. E-mail: wang_j_a@yahoo.com.

† Member of El Colegio Nacional, Mexico.

10.1021/jp0044429 CCC: $20.00
Published on Web 09/13/2001

TABLE 1: Atomic Fraction Coordinates of Fe_2TiO_5[a]

atom	sites	*x*	*y*	*z*
1 Ti	4c	0.190	0.250	0.000
1 Fe	8f	0.135	0.560	0.000
1 O	4c	0.730	0.250	0.000
2 O	8f	0.045	0.110	0.000
3 O	8f	0.310	0.095	0.000

[a] The unit cell is with monoclinic space group *BBMM*.

to 600 °C, titania reacts with iron ions to produce titanium−iron solid solution or Fe_xTiO_y ($FeTiO_3$ or Fe_2TiO_5).[19−21] Due to the migration of metallic cations and due to dehydroxylation during the thermal treatment, some special structural defects may be created when the catalysts are prepared by using a sol−gel technique. Recently, some studies have emphasized the relationship between catalytic activity and defect structure of pure or doped catalysts.[22−27] Unfortunately, the quantitative determination of the structural defects in the crystals is difficult due to the lack of reliable computer simulation techniques.

In the current work, several iron−titanium oxides with different iron contents prepared with a sol−gel technique were studied, using X-ray diffraction technique together with Rietveld simulation. Dehydroxylation of the dried sample was characterized by using FTIR. Solid-state reaction mechanisms and phase transformations were explored. The crystalline structures of all the samples calcined at different temperatures were refined with Rietveld technique, to obtain average crystallite size, lattice cell parameters, phase compositions, and cationic defect concentrations quantitatively.

2. Experimental Section

2.1. Preparation of the Catalyst Samples. Fe/TiO_2 samples were prepared by using a sol−gel technique. A typical preparation procedure, for 1 wt % Fe/TiO_2, is as follows: 0.045 g of $FeCl_2$ was dissolved in a mixture of 16.1 mL of water and 50 mL of ethanol. Afterward, 0.4 mL of 98% concentrated hydrochloric acid was used as a hydrolysis catalyst to add to this solution for controlling pH at 3. Then 84.5 mL of Ti(*n*-OBu)$_4$ was slowly dropped into the above solution, and the mixture was refluxed for 3 h at 70 °C with continuous stirring. Finally, the resulting materials were dried at 80 °C for 10 h and then calcined at 200, 400, 600, and 800 °C for 4 h, respectively.

2.2. FTIR Studies. The dried gel samples were characterized by FTIR spectroscopy by using a Perkin-Elmer 1600 spectrometer. Spectra were recorded after different heat treatments to characterize the surface dehydroxylization process.

2.3. X-ray Diffraction Analysis and Rietveld Refinement. XRD analyses were done at room temperature on a Siemens D-5000 diffractometer with Cu Kα radiation and secondary beam monochromator. The intensities were determined in the 5−110° of 2θ range with a 0.02° step size and measuring time of 2.7 s per point. The XRD patterns of the different samples calcined at different temperatures are presented in Figures1−6. The DBWS-9600PC and the WYRIET programs were applied to refine each spectrum using the Rietveld method.[28,29] The atomic fraction coordinates for brookite with space group *Pbca*, for anatase with space group *I41/amd* and rutile with space group *P42/mnm* are reported in a previous paper.[30] The atomic fraction coordinates for Fe_2O_3 and Fe_2TiO_5 are given in Tables 1 and 2. The average particle size and atomic occupancies in the different crystalline structures were obtained from their refinements. The standard deviations, showing the variation of the last figures of the corresponding number, are given in parentheses. When the numbers corresponded to parameters obtained from the Rietveld refinement, the estimated standard deviations are not estimates of the analysis as a whole but only of the minimum probable errors based on their normal distribution.

TABLE 2: Atomic Fraction Coordinates of Hematite[a]

atom	sites	*X*	*Y*	*Z*
1 Fe	4c	0.355	0.355	0.355
1 O	2b	0.000	0.000	0.000

[a] The unit cell is tetragonal with space group R-3C.

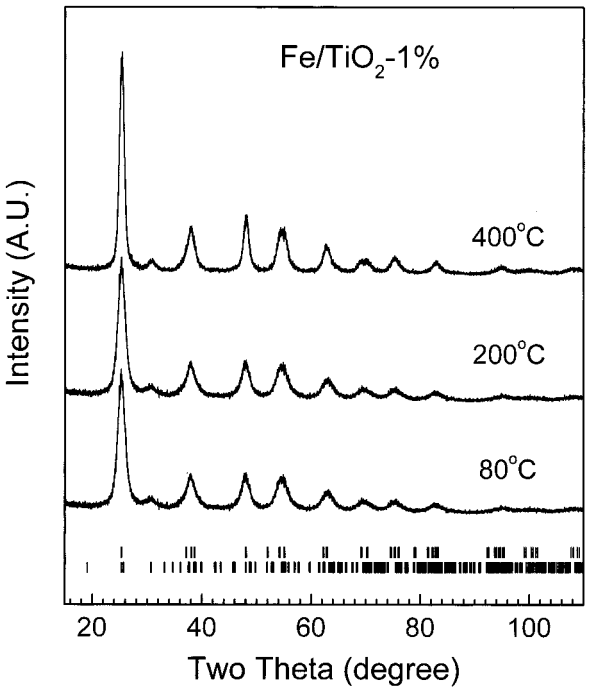

Figure 1. XRD patterns of the Fe/TiO_2-1 sample calcined at 70, 200, and 400 °C. The upper tick marks correspond to anatase, and the lower tick marks correspond to brookite.

3. Results and Discussion

3.1. Solid-State Reaction Mechanisms and Phase Transformation. In the Fe/TiO_2-1 (1 wt % Fe) sample calcined at 80 °C, both anatase and brookite were formed. When the calcination temperature was increased to 200 °C and 400 °C, since the XRD spectra remained almost unchanged except for a slight increase in intensity of the diffraction lines, no significant structure change occurred (Figure 1). At 600 °C calcination, however, this sample underwent phase transformation: the brookite phase disappeared, and the rutile crystalline phase coexisting with anatase was produced (Figure 2). This result shows that phase transformation from brookite to rutile takes place in the temperature range between 400 and 600 °C. When the calcination temperature reached 800 °C, only rutile existed, showing that anatase was also completely transformed into rutile.

It is noteworthy that iron oxides or Fe_xTiO_y phases were not formed in this sample in the temperature between 80 and 800 °C. We assumed that all the iron ions were inserted into the structures of titania and located at interstices or occupied some of the titanium lattice sites, forming an iron−titanium solid solution.

In the Fe/TiO_2-5 (5 wt % Fe) sample, below 400 °C calcination, similar to the sample Fe/TiO_2-1, anatase and

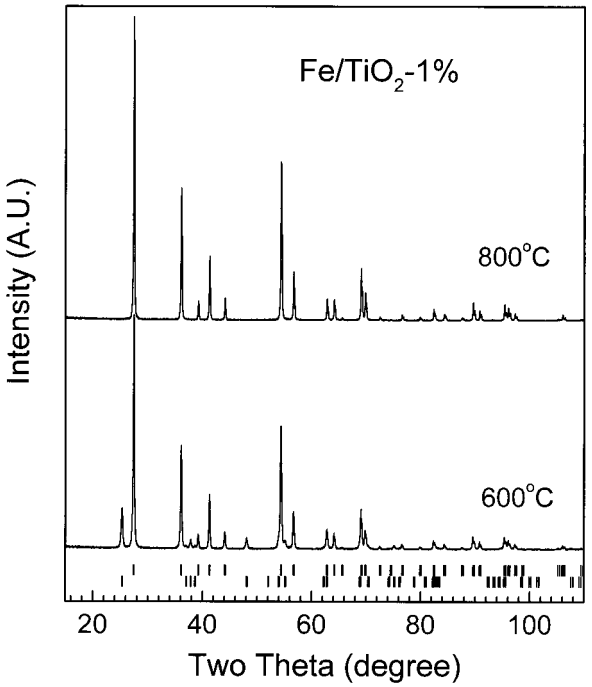

Figure 2. XRD patterns of the Fe/TiO_2-1 sample calcined at 600 and 800 °C. The upper tick marks correspond to rutile, and the lower tick marks correspond to anatase.

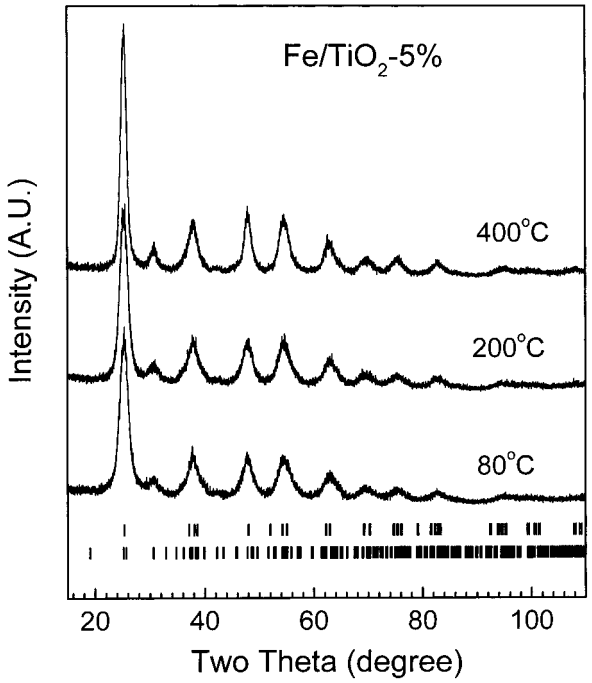

Figure 3. XRD patterns of the Fe/TiO_2-5 sample calcined at 70, 200, and 400 °C. The upper tick marks correspond to anatase, and the lower tick marks correspond to brookite.

brookite phases coexisted (Figure 3). However, unlike the Fe/TiO_2-1 sample where anatase existed together with rutile after 600 °C calcination, this sample had three phases—brookite, anatase, and rutile at 600 °C (Figure 4). When the calcination temperature was increased to 800 °C, the brookite phase disappeared and one new phase, pseudo-brookite (Fe_2TiO_5), was formed. Because iron oxide was not produced below 800 °C calcination, as we suggested above, these iron ions probably inserted into the structures of titania, forming a titanium−iron solid solution. Therefore, at 800 °C, an Fe_2TiO_5 crystal was

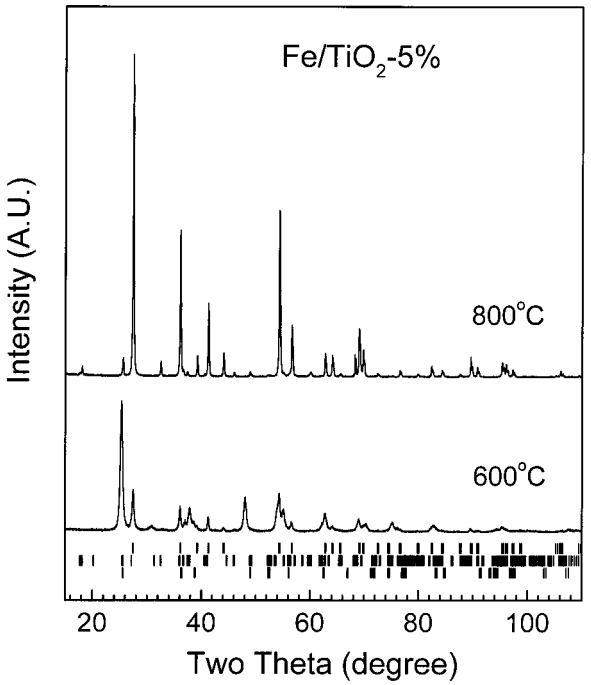

Figure 4. XRD patterns of the Fe/TiO_2-5 sample calcined at 600 and 800 °C. The upper tick marks correspond to rutile, the middle tick marks correspond to pseudobrookite, and the third tick marks correspond to anatase.

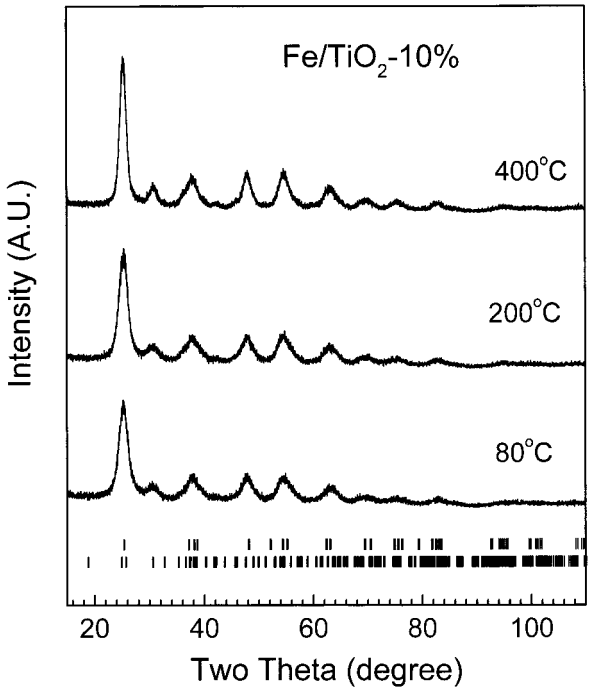

Figure 5. XRD patterns of the Fe/TiO_2-10 sample calcined at 70, 200, and 400 °C. The upper tick marks correspond to anatase and the lower tick marks correspond to brookite.

produced by means of titania reacting with the iron ions in a form of solid solution (referred as $TiO_2(Fe^{3+})$):

$$TiO_2(2Fe^{3+}) + 3O^{2-} \rightarrow Fe_2TiO_5 \quad (1)$$

In the Fe/TiO_2-10 (10 wt % Fe) sample, anatase and brookite phases were formed when it was calcined at 80, 200, and 400 °C (Figure 5). Similar to the Fe/TiO_2-1 and Fe/TiO_2-5 samples,

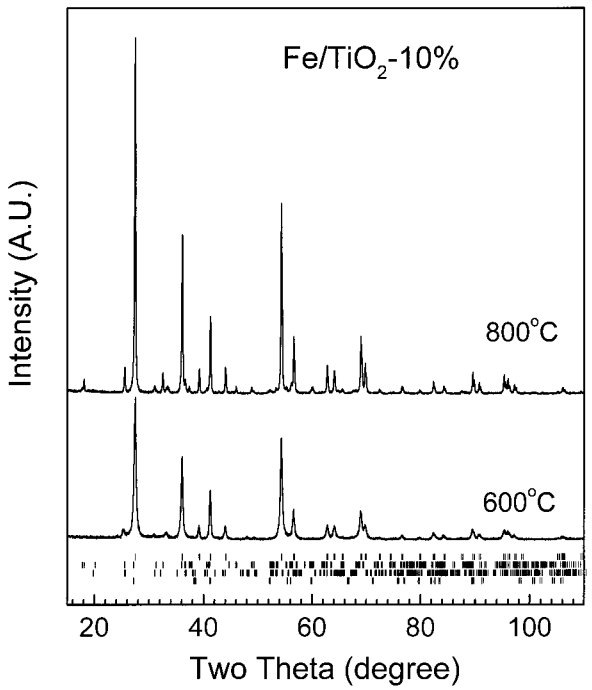

Figure 6. XRD patterns of the Fe/TiO_2-10 sample calcined at 600 and 800 °C; The upper tick marks correspond to rutile, the second tick marks correspond to pseudobrookite, the third tick marks corresponded to hematite, and the lowest tick marks correspond to anatase.

below 400 °C calcination, iron ions existed in a solid solution with titania like $TiO_2(Fe^{3+})$. However, differing from the Fe/TiO_2-1 and Fe/TiO_2-5 samples, this sample calcined at 600 °C had a hematite phase (Fe_2O_3), separate from titania phases (Figure 6).

Since the precursor of iron is $FeCl_2$, during the preparation and calcination in air, Fe^{2+} ions were easily oxidized to Fe^{3+} ions (eq 2):

$$Fe^{2+} \rightarrow Fe^{3+} + e \quad (2)$$

These Fe^{3+} ions reacted with oxygen anions to form the Fe_2O_3 phase (eq 3):

$$TiO_2\,(2Fe^{3+}) + 3O^{2-} \rightarrow TiO_2 + Fe_2O_3 \quad (3)$$

When the Fe/TiO_2-10 sample was fired at 800 °C, both anatase and brookite were partially transformed into rutile. Because hematite disappeared and a new phase Fe_2TiO_5 appeared at 800 °C, therefore, Fe_2TiO_5 crystal in this sample was produced by titania reacting with Fe_2O_3.

$$TiO_2 + Fe_2O_3 \rightarrow Fe_2TiO_5 \quad (4)$$

These different mechanisms of solid-state reactions and phase transformations occurring in the three samples are illustrated in Scheme 1.

3.2. Effects of Calcination Temperature and Iron Content. The calcination temperature shows remarkable effect on the solid-state reaction and phase transformation. Tables 3 through 5 give the information concerning phase concentration in each sample calcined at different temperatures. Below 400 °C calcination, all the samples had anatase and brookite crystals with anatase phase (>80 wt %). When the calcination temperature reached 800 °C, pseudobrookite with a concentration less than 8 wt % was formed. At 800 °C, in the sample containing

TABLE 3: The Concentration of Each Phase in Fe/TiO_2-1 Sample Calcined at Different Temperatures

calcd temp. (°C)	phase concentration (wt %)		
	anatase	brookite	rutile
70	89.9	10.1	
200	89.7	10.3	
400	88.0	12.0	
600	14.2		85.8
800			100.0

TABLE 4: The Concentration of Each Phase in Fe/TiO_2-5 Sample Calcined at Different Temperatures

calcd temp. (°C)	phase concentration (wt %)			
	anatase	brookite	rutile	pseudobrookite
70	88.1	11.9		
200	86.9	13.1		
400	86.8	13.2		
600	70.8	43.9	25.3	
800	3.2		90.3	6.5

TABLE 5: The Concentration of Each Phase in Fe/TiO_2-10 Sample Calcined at Different Temperatures

calcd temp. (°C)	phase concentration (wt %)				
	anatase	brookite	rutile	hematite	pseudobrookite
70	86.6	13.4			
200	82.7	17.3			
400	80.3	19.7			
600	1.8	5.5	89.3	3.4	
800	1.2	3.2	87.6		8.0

1 wt % Fe, 100% of rutile crystal was obtained. However, for the other two samples, approximately 85 wt % rutile, together with other phases, was formed.

The average crystallite size was nanoscale from 4 to 10 nm when the calcination temperature was below 400 °C (Tables 6−8). As the calcination temperature increased to 600 and 800 °C, accompanying the phase transformation from anatase and brookite to rutile, the crystallite size of the phases increased.

As discussed above, iron content also strongly impacts phase transformation. When the iron content was greater than 5 wt %, hematite phase was formed and separated from the Ti−Fe−O solid solution. At 800 °C, hematite reacted with titania to produce Fe_2TiO_5 crystals.

It is reported that formation of separate phases Fe_2O_3 and Fe_2TiO_5 results in a decrease of photocatalytic activity because of the transformation of charge carriers from TiO_2 to Fe_2O_3 or Fe_2TiO_5.[31] Increasing either or both the iron content and the calcination temperature leads to the formation of additional phases. Moreover, the surface area decreases due to the formation of rutile at high temperature. Therefore, it is important to calcine the samples below 600 °C and control iron content less than 5 wt % for the iron-doped titania photocatalysts.

The lattice cell parameters of three titania structures changed with iron content and calcination temperature (Tables 9−12). For example, in anatase in the 5% Fe sample, when the calcination temperature increased, lattice cell parameter *a* decreased; however, in contrast, cell parameter *c* decreased. The lattice cell distortion is large in the sample calcined at 800 °C.

3.3. Cationic Defects in the Crystalline Structures. We particularly refined the cation occupancies in the crystal structures of titanium oxides in the samples. Figures 7−9 show the Rietveld refinement plots of the different samples calcined at different temperatures. Due to the very small crystallite particles and small phase concentration in brookite, we did not refine its atomic occupancy. In the three samples, titanium

SCHEME 1: Mechanism of the Solid State Reactions in the Samples Calcined at Different Temperatures.T_A: Anatase; T_B: Brookite; T_R: Rutile. The Black Points Inside the Circles Are Representative of the Iron Ions Present in the Structures of Titania. The Concentrations of Different Phases Are Roughly Illustrated by the Area of the Circles

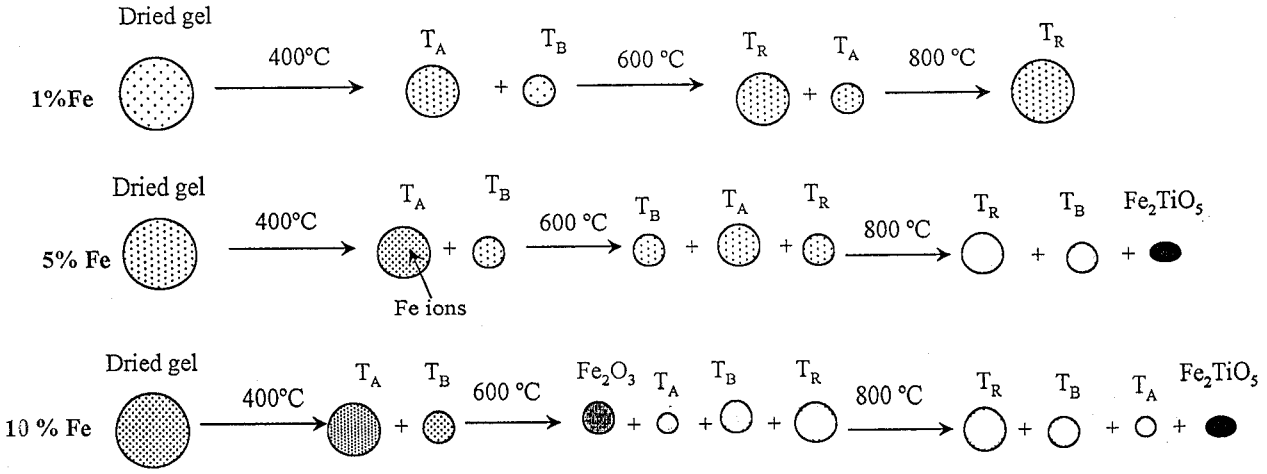

TABLE 6: Average Crystallite Size (nm) of the Phases in the Fe/TiO_2-1 Sample Calcined at Different Temperatures

calcd temp. (°C)	anatase	brookite	rutile
70	7.0(2)	7.5(2)	
200	7.2(3)	8.30(3)	
400	12.7(5)	18(3)	
600	45(3)		63(1)
800			106(2)

TABLE 7: Average Crystallite Size (nm) of Different Phases in the Sample Fe/TiO_2-5 Calcined at Different Temperatures

calcd temp. (°C)	anatase	brookite	rutile	pseudobrookite
70	5.1(2)	6.9(0)		
200	7.1(3)	7.6(8)		
400	11.9(5)	10.6(3)		
600	26.4(9)	17(1)	30(2)	
800	78(4)		79(2)	65(15)

TABLE 8: Average Crystallite Size (nm) of Different Phases in the Sample Fe/TiO_2-10 Calcined at Different Temperatures

calcd temp. (°C)	anatase	brookite	rutile	hematite	pseudobrookite
70	4.4(3)	8.2(1)			
200	5.3(3)	8.6(3)			
400	9.2(7)	8.8(1)			
600	9.4(5)		26.4(0)	67(2)	
800	77.4(1)		68(2)		69(16)

TABLE 9: Lattice Cell Parameters of Anatase as a Function of Iron Content

calcd temp. (°C)	lattice cell parameters (Å)					
	Fe/TiO_2-1		Fe/TiO_2-5		Fe/TiO_2-10	
	a	*c*	*a*	*c*	*a*	*c*
70	3.787(9)	9.459(3)	3.789(1)	9.440(4)	3.788(2)	9.436(6)
200	3.789(1)	9.460(4)	3.787(1)	9.454(4)	3.788(2)	9.449(5)
400	3.784(1)	9.463(2)	3.786(1)	9.456(3)	3.787(1)	9.439(4)
600	3.782(1)	9.508(1)	3.783(1)	9.498(1)	3.782(2)	9.456(2)
800			3.716(4)	9.902(8)	3.501(1)	9.405(4)

occupancy in the structures of anatase and rutile phases is less than its stoichiometric number 0.125, indicating that titanium atoms are deficient in the crystal structures. The refinement results are shown in Tables 13 and 14.

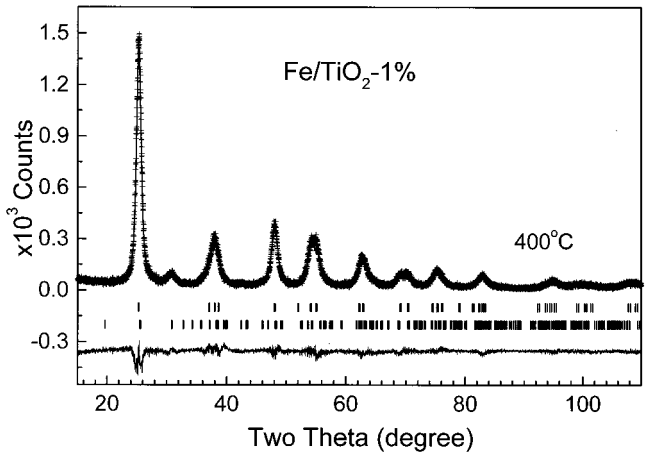

Figure 7. Rietveld refinement plot of the Fe/TiO_2-1 sample calcined at 400 °C; Experimental data are indicated by crosses while the calculated curve obtained after the refinement is indicated with a continuous line. The upper and lower tick marks, respectively, correspond to anatase and brookite phase. The continuous curve under the tick marks represents the difference between the experimental data and the calculated curve.

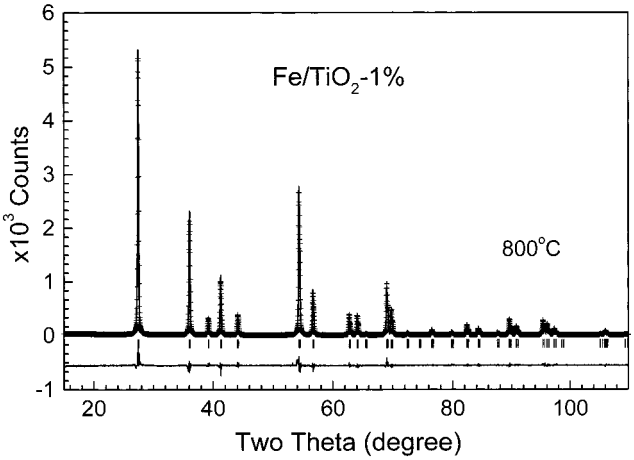

Figure 8. Rietveld refinement plot of the Fe/TiO_2-1 sample calcined at 800 °C. Experimental data are indicated by crosses while the calculated curve obtained after the refinement is indicated with a continuous line. The tick marks correspond to rutile. The continuous curve under the tick marks represents the difference between the experimental date and the calculated curve.

TABLE 10: Lattice Cell Parameters of Brookite as a Function of Iron Content

calcd temp. (°C)	lattice cell parameters (Å)								
	Fe/TiO_2-1			Fe/TiO_2-5			Fe/TiO_2-10		
	a	*b*	*c*	*a*	*b*	*c*	*a*	*b*	*c*
70	9.297(1)	5.409(2)	5.164(6)	9.101(9)	5.422(5)	5.179(4)	9.29(1)	5.439(5)	5.1748(4)
200	9.308(16)	5.12(7)	5.169(5)	9.303(1)	5.445(6)	5.159(5)	9.29(1)	5.444(5)	5.183(4)
400	9.007(9)	5.455(4)	5.227(3)	9.263(9)	5.461(4)	5.157(3)	9.15(1)	5.473(4)	5.167(4)
600				9.124(1)	5.427(7)	5.171(5)	9.26(2)	5.43(1)	4.98(1)
800							8.953(1)	5.573(5)	5.098(7)

TABLE 11: Lattice Cell Parameters of Rutile

samples	lattice cell parameters (Å)			
	600 °C		800 °C	
	a	*c*	*a*	*c*
Fe/TiO_2-1			4.5901(1)	2.9583(1)
Fe/TiO_2-5	4.5916(3)	2.9584(3)	4.9503(1)	2.9578(1)
Fe/TiO_2-10	4.9529(1)	2.9592(1)	4.9511(1)	2.9575(1)

TABLE 12: Lattice Cell Parameters (Å) of Psuedobrookite at 800 °C

calcd temp. (°C)	*a*	*b*	*c*
800	9.791(2)	9.972(2)	3.7225(5)

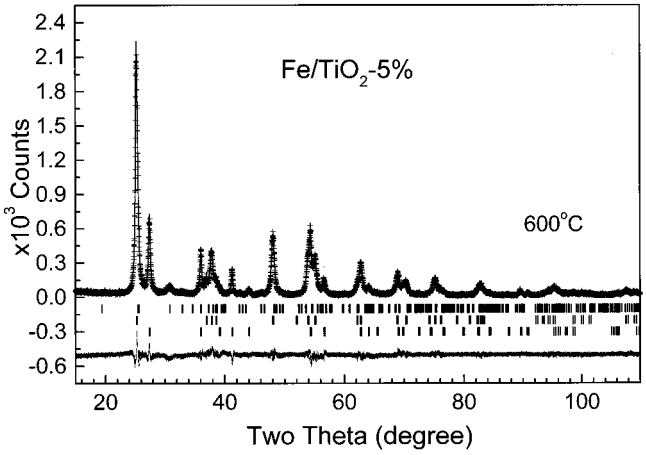

Figure 9. Rietveld refinement plot of the Fe/TiO_2-5 sample calcined at 600 °C. Experimental data are indicated by crosses, while the calculated curve obtained after the refinement is indicated with a continuous line. The upper tick marks correspond to brookite, the middle tick marks correspond to anatase, and the lowest tick marks correspond to rutile. The continuous curve under the tick marks represents the difference between the experimental data and the calculated curve.

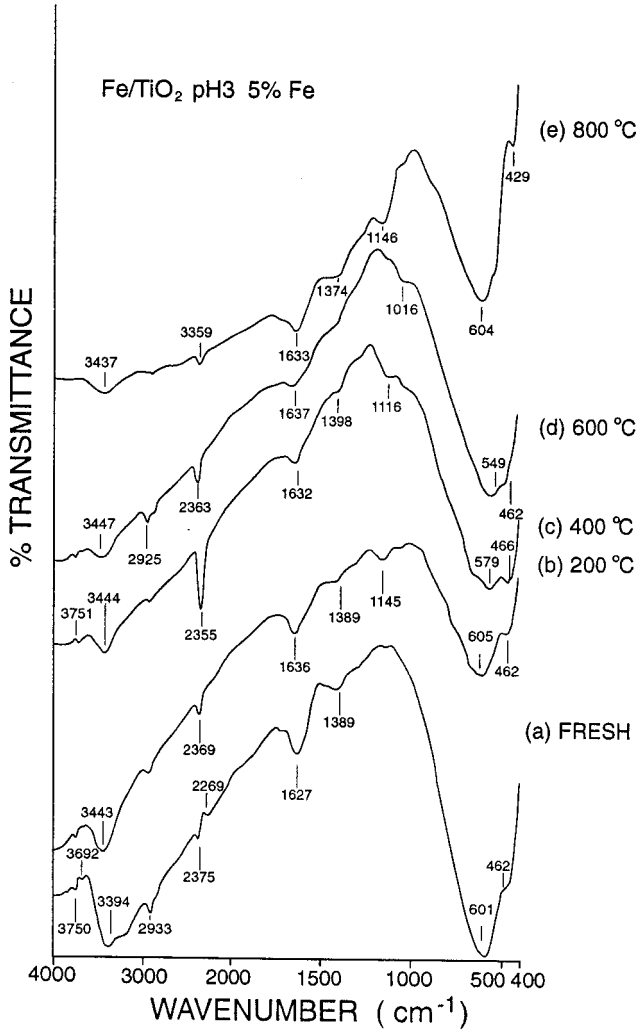

Figure 10. A set of FTIR spectra of the sample Fe/TiO_2-5 calcined at 80, 200, 400, 600, and 800 °C.

It was observed from Table 13 that iron content strongly affects the titanium defect concentration. When iron content increased, the titanium defect concentration increased. For example, at 400 °C, when iron content increased from 1 to 5 and 10 wt %, the concentration of titanium defects per unit cell in anatase increased from 16.8% in Fe/TiO_2-1 to 20.2% in Fe/TiO_2-5 and 23.4% in Fe/TiO_2-10.

The calcination temperature also shows an important effect on the defect formation. Below 400 °C, titanium defect concentration remained almost unchanged. However, when the temperature increased from 400 to 600 °C, the defect concentration was remarkably decreased.

Compared to anatase, titanium defect concentration in the structure of rutile is relatively low (Table 14). Also the effect of iron content is not significant since the defect concentration did not change with the iron concentration.

In the stages of hydrolysis and condensation during the sample preparation, many hydroxyl ions and molecular water existed. When the samples were calcined at low temperature, e.g., below 400 °C, the adsorbed water molecules were desorbed from the surface. As the calcination temperature continued to increase, the retained hydroxyl ions react with their adjacent hydroxyl ions to form water. At higher temperatures, most of hydroxyl ions in the structures disappeared and only very few percents of these ions remained in the structure of the samples according to FTIR (Figure 10). The calcination temperature, therefore, strongly impacted on the number of the residual OH ions and hence its crystalline structure.

A set of FTIR spectra of the sample Fe/TiO_2-5 calcined at 80, 200, 400, 600, and 800 °C are shown in Figure 10. Several bands corresponding to hydroxyls in the fresh sample were observed. The bands appearing at about 3750 cm^{-1} corresponded

TABLE 13: Titanium Defects of Anatase Structure in the Samples Calcined at Different Temperatures

temperature (°C)	titanium defects								
	Fe/TiO_2-1			Fe/TiO_2-5			Fe/TiO_2-10		
	O_n[a]	D_c[b]	D_n[c]	O_n[a]	D_c[b]	D_n[c]	O_n[a]	D_c[b]	D_n[c]
70	0.103(1)	18.3	0.73	0.099(2)	20.8	0.83	0.0929(2)	25.6	1.03
200	0.101(2)	19.2	0.76	0.0955(2)	23.6	0.94	0.0937(2)	25.0	1.00
400	0.104(1)	16.8	0.67	0.0977(1)	20.2	0.81	0.0958(2)	23.4	0.93
600	0.114(1)	8.8	0.35	0.1148(8)	8.2	0.33			

[a] O_n: titanium atomic occupancy number. [b] D_c: titanium defect concentration, in %. [c] D_n: titanium defect number in unit cell.

TABLE 14: Titanium Defects in Rutile Structure in the Samples Calcined at 800 °C

samples	titanium defects		
	O_n[a]	D_c[b]	D_n[c]
Fe/TiO_2-1	0.1151(8)	7.9	0.16
Fe/TiO_2-5	0.1147(6)	8.2	0.16
Fe/TiO_2-10	0.1146(7)	8.3	0.17

[a] O_n: Titanium atomic occupancy number; [b] D_c: Titanium defect concentration, in %; [c] D_n: Titanium defect number in unit cell.

to the stretching vibration of OH groups linking with titanium atoms Ti−OH and the wide band at 3394 cm^{-1} is responsible for the OH^- in water adsorbed in the sample (Figure 10a). The small absorption band at 2933 cm^{-1} is probably caused by the stretching mode of unreacted ethoxy groups such as $-Ti-OCH_2CH_3$.[32] Another band corresponding to O−H flexion vibration was also observed at 1627 cm^{-1}. The band centered at 1389 cm^{-1} is assigned to bending vibrations of C−H bond in the species linking −Ti−O−Ti− structural network. In the region below 1000 cm^{-1}, several peaks were ascribed to absorption bands of Ti−O and O−Ti−O flexion vibration. These results strongly confirm the presence of hydroxyl ions in the structure of the samples.

When the calcination temperature increased, the intensities of the various bands related to hydroxyls were obviously decreased, indicating that the hydroxyl ions gradually diminished. However, even the sample calcined at 800 °C has the bands corresponding to OH^- (Figure 10e). These results show that the structural network still retains some hydroxyls. The FTIR results are in good agreement with the XRD analysis and Rietveld refinements.

4. Conclusions

This work illustrated how computer simulations combined with experimental techniques can contribute to explaining properties of iron-doped titania photocatalysts. It was found that iron content and calcination temperature are essential to the formation of titanium cation defects and phase transformation. Below 400 °C calcination, titanium−iron solid solutions were formed. When the samples were calcined up to 800 °C, pseudobrookite was produced through different pathways: for the sample containing 10 wt % Fe, by a reaction of hematite with titania crystals, and for the sample with 5 wt % Fe, by a reaction between iron ions occupying lattice sites in the crystal structure and titanium ions. In the 1 wt % Fe sample, however, iron ions were uniformly distributed in titania phases in the temperature ranging 70 to 800 °C.

The formation of titanium lattice defects in the crystal structures of titania phases can be explained by compensation for the extra hydroxyl ions present in the crystal structures. The population of titanium defects in the crystals remained almost unchanged below 400 °C but decreased as calcination temperature increased up to 600 °C.

Acknowledgment. The authors thank the financial support from projects of CONACyT-31282-U (Mexico), FIES-98-29-III (IMP-IPN-Mexico), and CEGEPI-99-134 (IPN-Mexico).

References and Notes

(1) *Photoelectrochemistry, Photocatalysis and Photoreactors*; Schiavello, M., Ed.; Riedel: Dordrecht, 1985.

(2) Larson, S. A.; Widegren, J. A.; Falconer, J. L. *J. Catal*. **1995**, *157*, 611.

(3) Sabate, J.; Cervera-March, S.; Simarro, R.; Gimenez, J. *Int. J. Hydrogen Energy Prog*. **1990**, *15*, 115.

(4) Sabate, J.; Anderson, M. A.; Xu, H. Q.; Cervera-March, S.; Hill, C. G. *J. Catal*. **1992**, *134*, 36.

(5) Frank, T.; Ollis, D. F. *J. Phys. Chem*. **1984**, *88*, 3386.

(6) Ollis, D. F.; Hsiao, C.; Budiman, Y. L.; Lee, C. L. *J. Catal*. **1984**, *88*, 89.

(7) Tunesi, S.; Anderson, M. A. *Chemosphere* **1987**, *16*, 1447.

(8) Litter, M. I. *Appl. Catal. B: Environmental* **1999**, *23*, 89.

(9) Kim, K. S.; Barteau, M. A.; Farneth, W. E. *Langmiur* **1988**, *4*, 533.

(10) Peral, J.; Ollis, D. F. *J. Mol. Catal. A: Chemical* **1997**, *115*, 347.

(11) Serpone, N.; Borgarello, E.; Barbeni, M.; Pelizzetti, E. *Inorg. Chim. Acta* **1984**, *90*, 191.

(12) *Energy Resources through Photochemistry and Catalysis*; Graetzel, M., Ed.; Academic Press: New York, 1983.

(13) Wang, Y. Q.; Cheng, H. M.; Hao, Y. Z.; Ma, J.; Li, W. H.; Cai, S. M. *J. Mater. Sci*. **1999**, *34*, 3721.

(14) Pauling, L. *J. Am. Chem. Soc*. **1992**, *51*, 1010.

(15) Bokhimi, X.; Morales, A.; Novaro, O.; Lopez, T.; Sanchez, E.; Gómez, R. *J. Mater. Res*. **1995**, *10*, 2788.

(16) Navio, J. A. *J. Mater. Sci*. **1992**, *27*, 3036.

(17) Litter, M. I.; Navio, J. A. *J. Photochem. Photobiol. A: Chemical* **1994**, *98*, 183.

(18) Bickley, R. I.; Lettersal, J. S. *J. Chem. Soc., Faraday Trans*. **1994**, *88*, 377.

(19) Shirane, G.; Pickart, S. J.; Nathans, R.; Ishikawa, Y. *J. Phys. Chem. Solid* **1959**, *10*, 35.

(20) Gennari, F. C.; Andrade Gamboa, J. J.; Pasquevich, D. M. *J. Mater. Sci. Lett*. **1998**, *17*, 687.

(21) Drofenik, M.; Golic, L.; Hanzel, Krasevec, D. V.; Prodan, A.; Bakker, M.; Kolar, D. *J. Solid State Chem*. **1981**, *4*, 186.

(22) Llett, D. J.; Islam, S. *J. Chem. Soc., Faraday Trans*. **1993**, *89* (20), 3833.

(23) Kalenik, Z.; Wolf, E. E. *Catal. Lett*. **1992**, *9*, 283.

(24) Wang, J. A.; Novaro, O.; Bokhimi, X.; López, T.; Gómez, R. *J. Phys. Chem. B* **1999**, *103* (2), 299.

(25) Wang, J. A.; Novaro, O.; Bokhimi, X.; López, T.; Gómez, R. *J. Mol. Catal.* **1999**, *145*, 291.

(26) Wang, J. A.; Novaro, O.; Bokhimi, X.; López, T.; Gómez, R.; Navarrete, J.; Llanos, M. E.; López-Salinas, E. *J. Mol. Catal. A* **1999**, *137*, 239.

(27) Wang, J. A.; Novaro, O.; Bokhimi, X.; López, T.; Gómez, R.; Navarrete, J.; Llanos, M. E.; López-Salinas, E. *J. Phys. Chem. B* **1997**, *38* (101), 7448.

(28) Young, R. A.; Sakthivel, A.; Moss, T. S.; Paiva-Santos, C. O. *J. Appl. Crystallogr*. **1995**, *28*, 366.

(29) Margarita Schneider EDV-Vertrieb, Starnbergweg 18 D-8134, Pöcking, Germany, 1992, Tel: 0049-8157-8727; Fax 0049-8157-4527.

(30) Bokimi, X.; Morales, A.; Novaro, O.; Lopéz, T.; Gomez, R. *J. Mater. Res*. **1995**, *10* (11), 2788.

(31) Schrauzer, G. N.; Guth, T. D. *J. Am. Chem. Soc*. **1977**, *99*, 718.

(32) López, T.; García-Cruz, A.; Gómez, R. *J. Catal*. **1991**, *127*, 75.